Supporting Information for "Effects of increasing the resolution of the sea ice thickness distribution in a coupled climate model on Arctic and Antarctic sea ice"

Madison M. Smith[1], Marika M. Holland[2], Alek A. Petty[3], Bonnie Light[1],

David A. Bailey[2]

[1]Polar Science Center, Applied Physics Laboratory, University of Washington, Seattle, USA

[2]National Center for Atmospheric Research, Boulder, Colorado, USA

[3]Cryospheric Sciences Laboratory, NASA Goddard Space Flight Center, Greenbelt, MD, USA

Contents of this file

1. Figures S1 to S11

Introduction Figure S1 shows the change in sea ice thickness in both hemispheres in February associated with increasing the ITD category resolution from 5 to 15 categories. Figures S2 to S6 show comparisons of ITD histograms from model runs and ICESat-2 derived thicknesses for all other regions not included in the manuscript. Figures S7 to S11 show comparisons of the ITD mean annual cycle for all other regions not included in the manuscript.

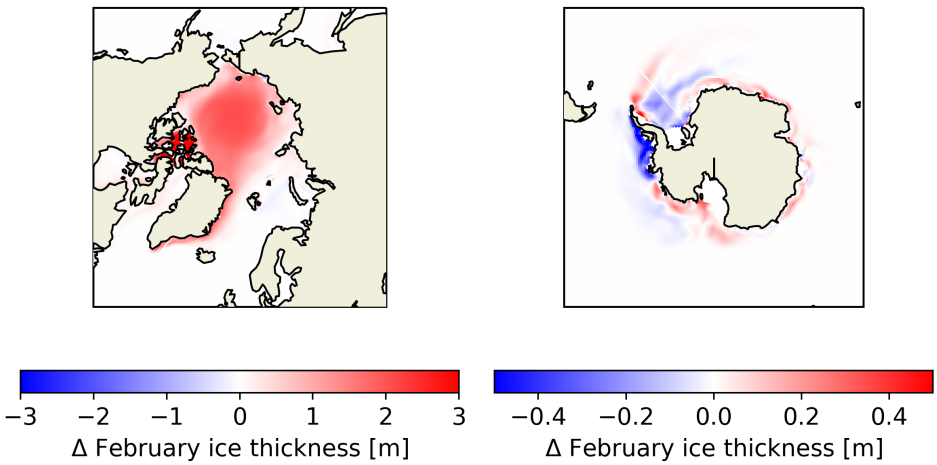

Figure S1. Difference in grid-averaged February sea ice thickness in the Arctic (left) and Antarctic (right) between run with 15 categories and 5 categories. Red indicates an increase in ice thickness with higher ITD category resolution, and blue indicates a decrease in ice thickness. Note that the scale of colorbar changes between panels.

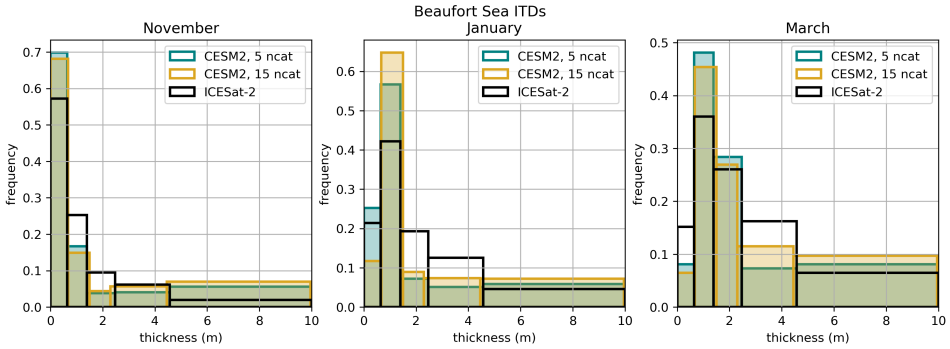

Figure S2. Comparison of discretized ice thickness distribution in the Beaufort Sea in model simulations and ICESat-2 for select months: November, January, and March. The average fraction of ice coverage in each category is shown for the 5 category model run (green), 15 category model run (gold), and ICESat-2 (black outline).

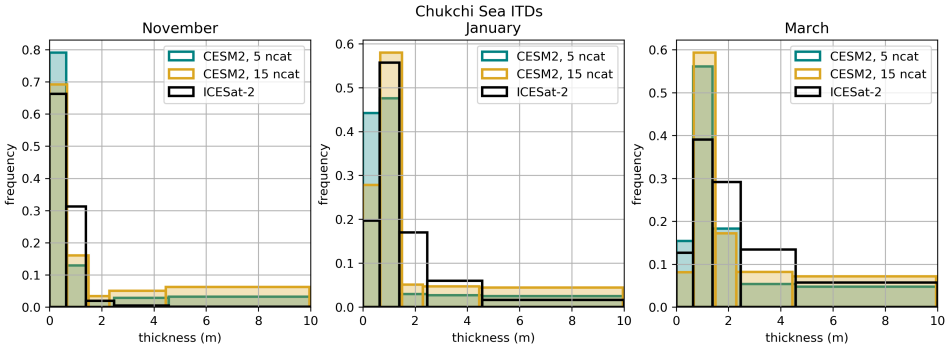

Figure S3. Comparison of discretized ice thickness distribution in the Chukchi Sea in model simulations and ICESat-2 for select months: November, January, and March. The average fraction of ice coverage in each category is shown for the 5 category model run (green), 15 category model run (gold), and ICESat-2 (black outline).

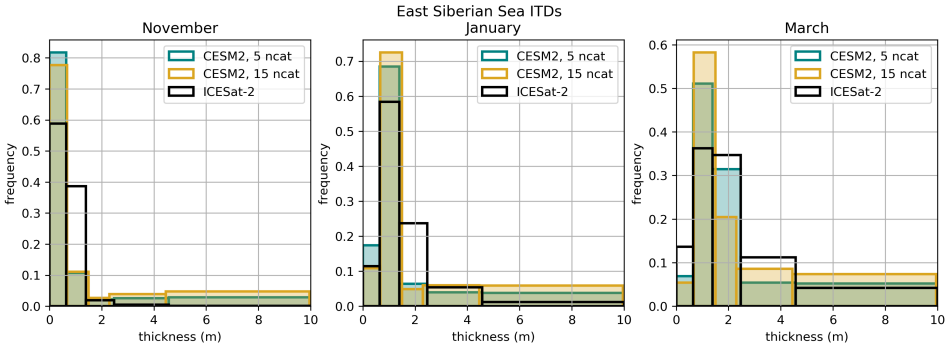

Figure S4. Comparison of discretized ice thickness distribution in the East Siberian Sea in model simulations and ICESat-2 for select months: November, January, and March. The average fraction of ice coverage in each category is shown for the 5 category model run (green), 15 category model run (gold), and ICESat-2 (black outline).

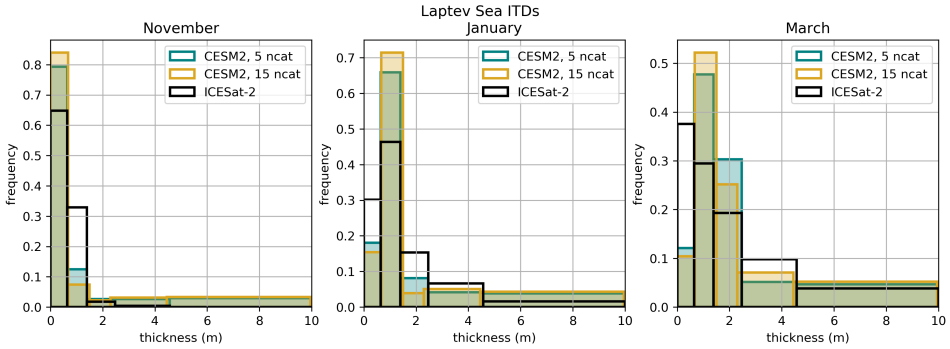

Figure S5. Comparison of discretized ice thickness distribution in the Laptev Sea in model simulations and ICESat-2 for select months: November, January, and March. The average fraction of ice coverage in each category is shown for the 5 category model run (green), 15 category model run (gold), and ICESat-2 (black outline).

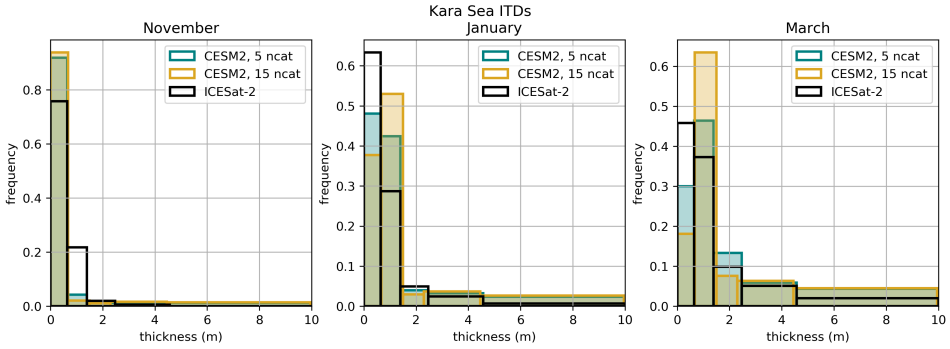

Figure S6. Comparison of discretized ice thickness distribution in the Kara Sea in model simulations and ICESat-2 for select months: November, January, and March. The average fraction of ice coverage in each category is shown for the 5 category model run (green), 15 category model run (gold), and ICESat-2 (black outline).

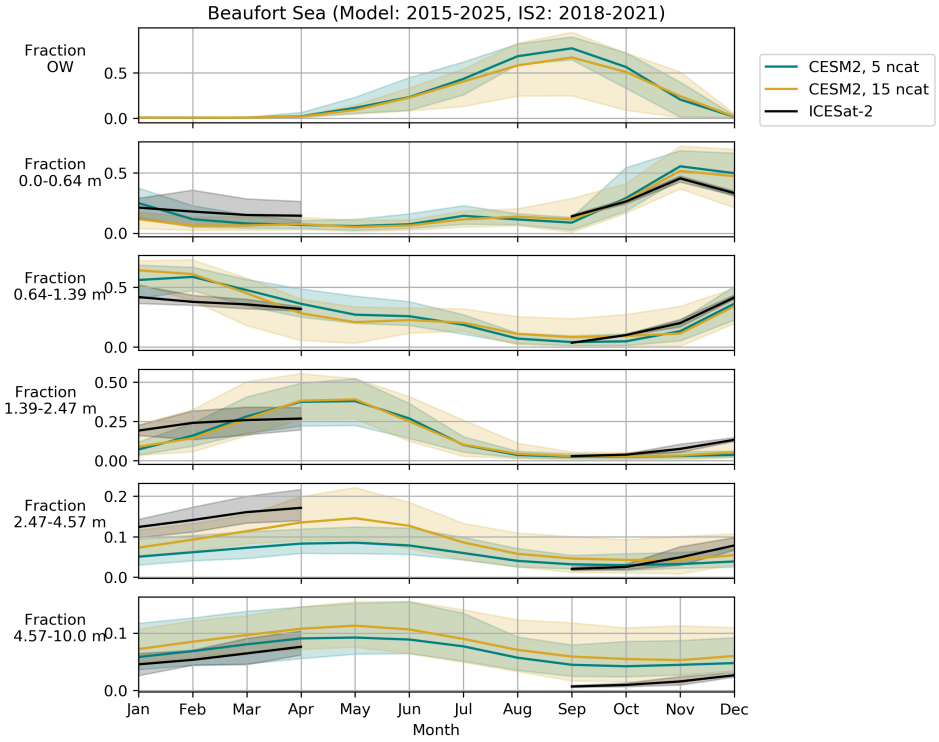

Figure S7. Mean annual cycle of the ice thickness distribution in the Beaufort Sea in model simulations and ICESat-2 observations. The fractional coverage of open water and in each ice category is shown for the control 5 category model run (green), 15 category model run (gold), and ICESat-2 (black). Shading represents the full range of values over the 10 years analyzed from the model or the 3 years of observations.

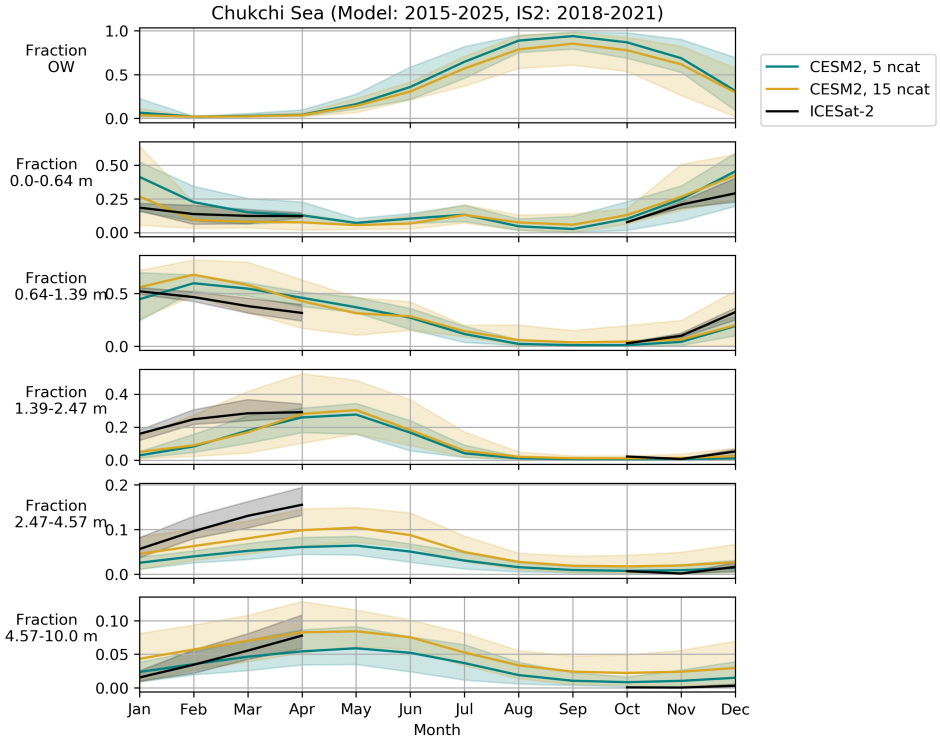

Figure S8. Mean annual cycle of the ice thickness distribution in the Chukchi Sea in model simulations and ICESat-2 observations. The fractional coverage of open water and in each ice category is shown for the control 5 category model run (green), 15 category model run (gold), and ICESat-2 (black). Shading represents the full range of values over the 10 years analyzed from the model or the 3 years of observations.

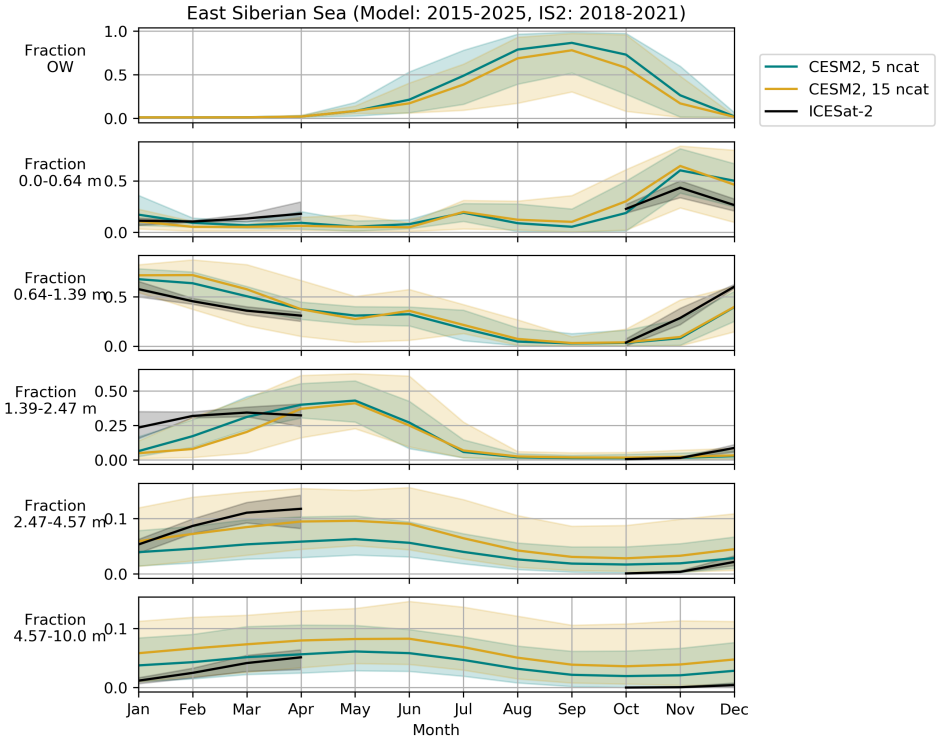

Figure S9. Mean annual cycle of the ice thickness distribution in the East Siberian Sea in model simulations and ICESat-2 observations. The fractional coverage of open water and in each ice category is shown for the control 5 category model run (green), 15 category model run (gold), and ICESat-2 (black). Shading represents the full range of values over the 10 years analyzed from the model or the 3 years of observations.

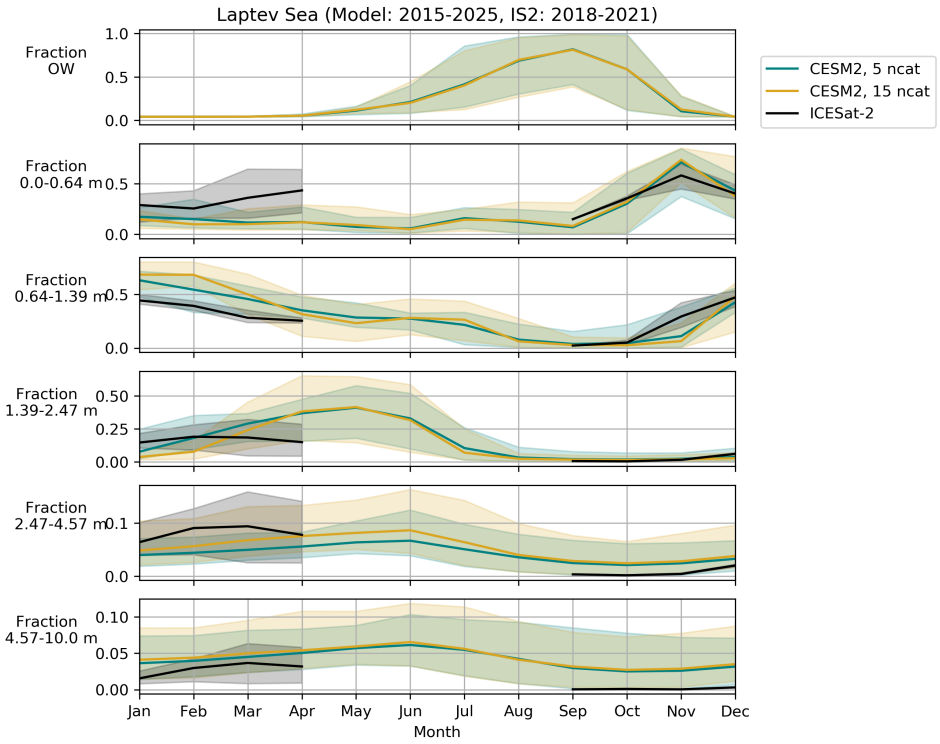

Figure S10. Mean annual cycle of the ice thickness distribution in the Laptev Sea in model simulations and ICESat-2 observations. The fractional coverage of open water and in each ice category is shown for the control 5 category model run (green), 15 category model run (gold), and ICESat-2 (black). Shading represents the full range of values over the 10 years analyzed from the model or the 3 years of observations.

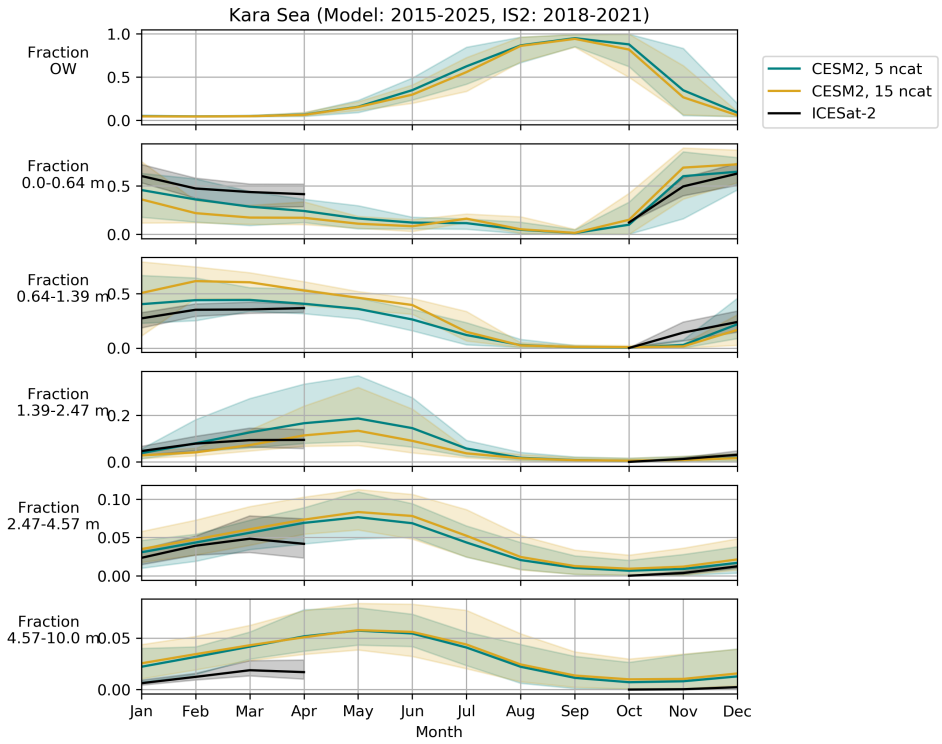

Figure S11. Mean annual cycle of the ice thickness distribution in the Kara Sea in model simulations and ICESat-2 observations. The fractional coverage of open water and in each ice category is shown for the control 5 category model run (green), 15 category model run (gold), and ICESat-2 (black). Shading represents the full range of values over the 10 years analyzed from the model or the 3 years of observations.